Journal of Soil Salinity and Water Quality 17(2), 119-128, 2025
DOI: https://doi.org/10.56093/jsswq.v17i2.168350

3D Mapping of Soil Salinity in Sub-surface Drainage Project Site Using Electromagnetic Induction (EMI) and Inversion Modelling

Bhaskar Narjary*, Raj Mukhopadhyay, Arijit Barman and DS Buldela

ICAR-Central Soil Salinity Research Institute, Karnal-132001, Haryana, India
**Corresponding author's E-mail: bhaskar.narjary@gmail.com*

Abstract

Soil salinity is a significant form of chemical land degradation, impeding crop productivity and sustainability in irrigated and arid regions. Traditional two-dimensional (2D) soil salinity maps are limited in scope, lacking critical vertical salinity distribution data necessary for effective reclamation planning. This study aimed to generate a three-dimensional (3D) soil salinity map using electromagnetic induction (EMI) techniques and inversion modeling at subsurface drainage (SSD) site in Kahni village, Rohtak, Haryana, India. Soil apparent electrical conductivity (EC_a) was measured using the EM38MK2 sensor in both vertical and horizontal orientations at two depth responses (0.5 m and 1 m) across two experimental blocks: Block 1 (B1, non-continuous SSD operation) and Block 2 (B2, continuous SSD operation). 3D inversion algorithm (EM4Soil) was applied to estimate true soil conductivity (σ), which was then correlated with electrical conductivity of saturated paste extract (EC_e). The developed regression model ($ECe = 1.024 + 0.0460\ \sigma$, $R^2 = 0.71$) showed strong predictive ability (RMSE = 5.03 dS m^{-1}; Lin's concordance = 0.84). The resulting 3D salinity maps revealed that continuous SSD operation significantly reduced salinity in B2 across all depths and minimized spatial variability, whereas B1 showed persistent high salinity due to inadequate drainage. Deeper layers in both blocks had higher salinity, indicating salt leaching from surface soils. This study demonstrates the effectiveness of EMI and inversion modeling for 3D salinity assessment, offering a rapid, non-destructive, and cost-effective tool for precision land and drainage management toward achieving Land Degradation Neutrality (LDN).

Keywords: Soil salinity, EM38MK2, EMI, 3D soil salinity mapping

Introduction

Among the different types of land degradation, soil salinity is one form of chemical land degradation. According to recent estimates by FAO (2024), salt-affected soil covers 10.7% of global land area. In India, salt-affected land covers 9.4% of the total land area (FAO, 2024). The global water cycle is projected to be hampered due to climate change, and soil salinization will increase in most of the continent (Hassani *et al.*, 2021; Vineeth *et al.*, 2023). Therefore, salinity mapping is essential for achieving the Land Degradation Neutrality (LDN) goal, as it provides spatial understanding of chemical land degradation, enabling targeted interventions and progress monitoring.

However, soil salinity is not uniformly distributed across a field and within the soil profile. It can vary depending on topographic, anthropogenic, parent material, climatic, and hydrologic factors. Soil salinity map is generally represented through 2-dimensional (2D) representation. However, it only shows the variation of soil salinity across a horizontal surface (at one fixed depth). The subsurface soil salinity information and its spatial variation are missing in 2D approach of soil salinity mapping. This limits the usefulness of the soil salinity map in real-world use, such as root zone salinity distribution, leaching efficiency, reclamation measures of subsurface drainage and future prediction of soil salinization over large areas. 3D soil salinity map captures horizontal and vertical salinity distribution.

Minimal studies, however, have been published on mapping 3D soil properties at a global level. Zhang *et al.* (2020) prepared digital

soil maps up to 1 m depth for volumetric water content, soil organic matter, and clay% using regression kriging (RK) with multiple proximal soil sensing techniques. Poggio and Gimona (2017) prepared a 3D soil texture map for Scotland at 250 m resolution. Jiang *et al.* (2019) characterized and prepared 3D dryland salinity map using EMI approach and an inversion algorithm.

Soil samples collection by traditional auger sampling methods (Carter and Gregorich, 2008) followed by determination of electrical conductivity of saturated paste extract (EC_e) is labour-intensive, expensive, and requires a longer period for assessment of soil salinity parameters. Electromagnetic induction (EMI) techniques, on the contrary, provide rapid, reliable, and non-destructive assessment and monitoring of surface and subsurface soil salinity (Narjary *et al.*, 2021; Vibhute *et al.,* 2024). EMI techniques provide bulk soil electrical conductivity (EC_a) at different depths (0.35, 0.75, 1.5, 2 m) depending on the number of transmitter coils and receiver coils in the instruments. The bulk soil electrical conductivity (EC_a) of different depth layers can be correlated with the Soil EC_e of the respective depth layer, and will help generate a dataset for mapping soil salinity 3-dimensionally with a suitable modelling technique.

The objective of the study is to develop a relationship between EC_a and EC_e across all depth layer (0-30, 30-60 and 60-90 cm) and prepare 3D soil salinity map through inversion modeling of EC_a data.

Material and Methods

Study area description

The field survey was conducted at a subsurface drainage (SSD) project site located in Kahni village, Rohtak district, Haryana, India. The study area falls in semi-arid region, with an average annual rainfall of approximately 500-600 mm. The study site is situated between longitudes 76.6760° E to 76.6900° E and latitudes 29.0020° N to 29.0140° N , and is underlain by saline groundwater. The soil was clay loam in texture across the site. In summer groundwater table ranges between 1.0 and 2.0 meters below ground level (bgl), and monsoon season, it ranges between 0.9 and 1.2 m bgl. For the reclamation of waterlogged and saline soil of the study site, a subsurface drainage system was implemented over 160 hectares across four blocks: Block 1 (B1), Block 2 (B2), Block 5 (B5), and Block 6 (B6) (Fig. 1). The SSD network was designed with lateral perforated pipes (80 mm diameter) spaced at 60 m intervals, which conveyed drainage water to

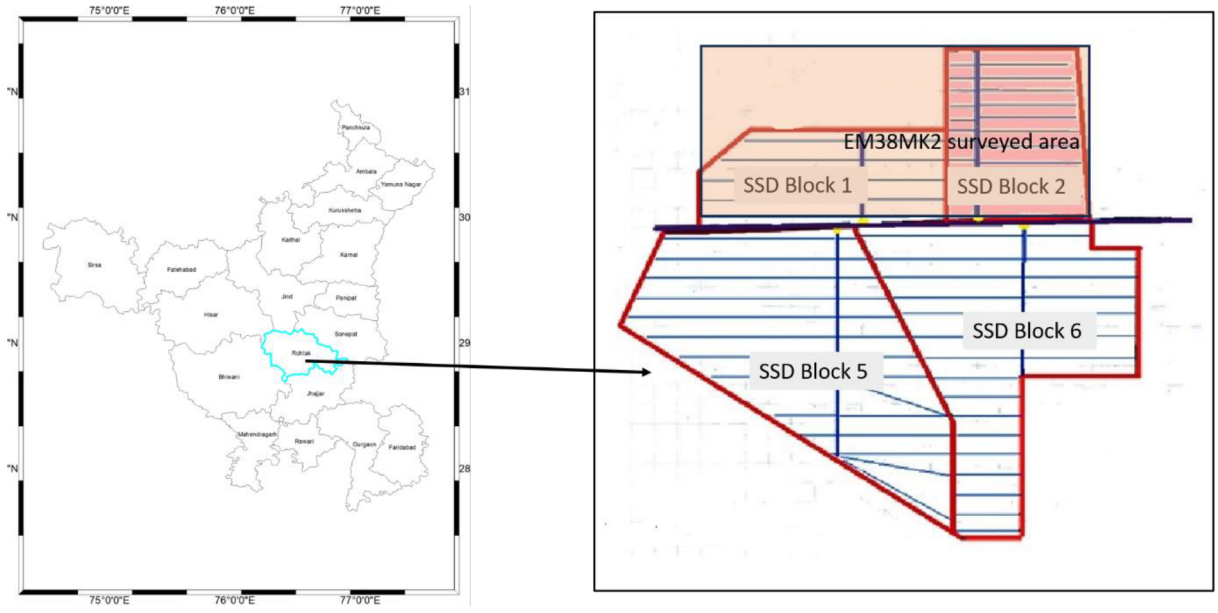

Fig. 1 Location of the study area (SSD block 1 and 2, Village : Kahni, District: Rohtak, Haryana)

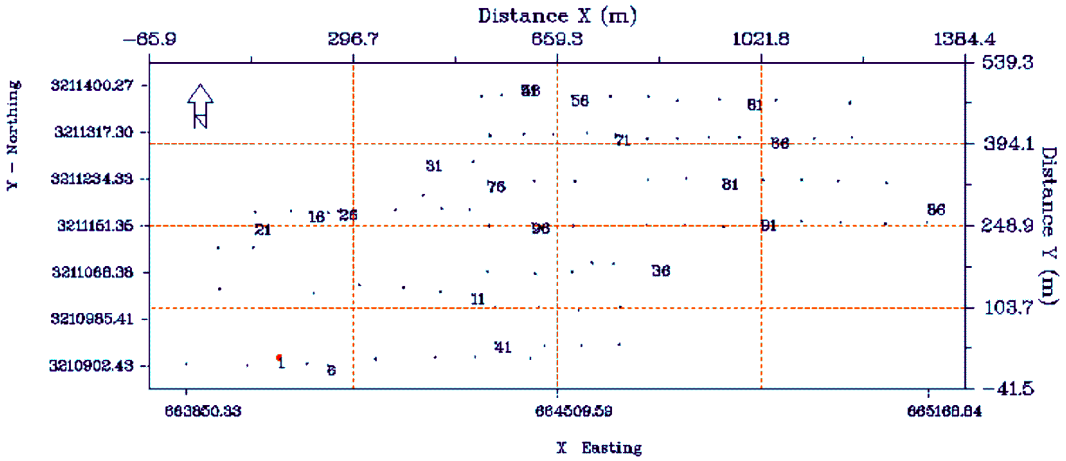

Fig. 2 EM38MK2 survey layout and Soil sample sites (Total survey points: 100; Soil sample sites: 16)

collector pipes (200 mm diameter). These collector drains transported the drainage effluent to designated sumps connected to a surface drain system. Drainage effluent from the sumps was discharged via pumping to ensure removal from the affected area.

Electromagnetic induction survey

Survey was conducted using EM38MK2, a proximal sensor for measuring soil salinity (Geonics Limited, Mississuaga, Canada) during April 2021 (Fig. 2). The EM38-MK2 electromagnetic induction (EMI) sensor is configured with a total of three electromagnetic coils: one transmitter (T_x) and two receiver (R_x) coils, enabling depth wise measurements of apparent electrical conductivity (EC_a) in soils (Geonics Limited, 2016). The transmitter coil, operating at a fixed frequency (~14.6 kHz), generates a primary electromagnetic field that induces eddy currents in the subsurface. These eddy currents, in response, produce a secondary magnetic field, which is detected by the receiver coils. The instrument incorporates two orthogonally oriented receiver coils to facilitate simultaneous multi-depth sensing. The horizontal dipole R_x coil, co-planar with the T_x coil, is sensitive to shallow subsurface layers with an effective depth of investigation up to 0.75 meters (maximum sensitivity between 0.3–0.5 m). The vertical dipole R_x coil, positioned perpendicular to the T_x coil, extends the sensing capability to a greater depth of approximately 1.5 meters, with peak sensitivity typically between 0.75-1.0 meters. This dual-receiver configuration permits concurrent acquisition of EC_a at distinct depth intervals from a single instrument orientation, and improving the spatial and vertical resolution of soil conductivity data (Petsetidi and Kargas, 2023). The survey was conducted in SSD block 1 (B1: Non-continuous dewatering) and block 2 (B2: continuous dewatering) along transects spaced ~50 m apart in a grid manner, and in total 100 survey points (apparent conductivity data: EC_a) were recorded (Fig. 2).

Soil sampling and laboratory analysis

For the calibration of apparent soil electrical conductivity (EC_a) with soil salinity (EC_e), a total of 16 sampling points were selected from the EMI survey grid (Fig. 2). Sampling sites were stratified based on the full range of EC_a values obtained from the EM38-MK2 survey and categorized into five classes: very low (<100 mS m^{-1}), low (100-200 mS m^{-1}), moderate (200-350 mS m^{-1}), high (350-500 mS m^{-1}), and very high (>500 mS m^{-1}). At each selected location, soil samples were collected from three depth intervals: surface (0-15 cm), subsurface (15-30 cm), and subsoil (30-90 cm), to capture vertical variation in salinity. The collected samples were air-dried, gently crushed, and passed through a 2 mm sieve before analysis. Soil salinity was measured by electrical conductivity of the saturated soil paste extract (EC_e) using a calibrated conductivity meter (Eutech Con 700, Eutech Instruments Pvt. Ltd., Singapore), following standard laboratory procedures as described by Yadav *et al.* (2015).

Apparent Conductivity (EC_a) data modelling: Inversion of data

Three-dimensional (3D) inversion was performed using EM4Soil software to generate 3D maps of salinity distribution within the study area. The inversion process employed a multi-level orthogonal model, utilizing the cumulative function (CF) algorithm for the calculation. The CF method, grounded in the concept of the apparent electrical conductivity (EC_a) cumulative response facilitates the transformation of depth-dependent conductivity profiles into EC_a values as described (McNeill, 1990; Zare *et al.*, 2015). In multilayers of subsurface models, the CF approach quantifies the relative contribution of each layer to the total electromagnetic response, thereby enhancing the resolution of conductivity variations with depth. The process flowchart of EC_a measurement in the field using EM38MK2 electromagnetic induction sensors and 3D map generation using EM4Soil is presented through Fig. 3.

Results and Discussion

Descriptive statistics

Table 1 represents the descriptive statistics of apparent conductivity (EC_a) measured by the EM38MK2 for Block1 (B1) and Block2 (B2) of sub-surface drainage (SSD) site (Kahni). EC_a was measured in Vertical and Horizontal mode at 0.5 and 1 m depth response. The mean EC_{av} (1 m) in B1 was 135.7 mS m^{-1} with a minimum of 35.5 mS m^{-1} and maximum of 496.4 mS m^{-1}. In contrast, at horizontal mode of same depth response EC_{ah} (1 m) had slightly lower mean (133.3 mS m^{-1}) and minimum (32.4 mS m^{-1}) but maximum was high (511.1 mS m^{-1}). The standard deviation (SD) in EC_{ah} (1m) was slightly greater (14.3) than EC_{av} (1 m) (14.2). At 0.5 m depth response, mean EC_{av} (0.5 m) in B1 was 122.7 mS m^{-1} with a minimum of 26.7 mS m^{-1} and maximum of 486.9 mS m^{-1}. The corresponding value in horizontal mode EC_{ah} (0.5 m) was 106.6 (mean) 16.1 (minimum) and 467.6 (maximum) mS m^{-1}.

In B2, mean values of vertical (EC_{av}) and horizontal (EC_{ah}) apparent conductivity in both 1 m and 0.5 m depth responses was lower than the B1. The mean EC_{av} (1 m) and EC_{av} (0.5 m) in B1 was 134.6 mS m^{-1} and 114.1 mS m^{-1}, while mean EC_{ah} (1m) and EC_{ah} (0.5 m) was 102.9 mS m^{-1} and 78.0 mS m^{-1}. These indicate that continuous SSD operation in B2 reduced soil salinity from the soil profile as compared to B1, where SSD operation was non-continuous. SSD operation removes salts

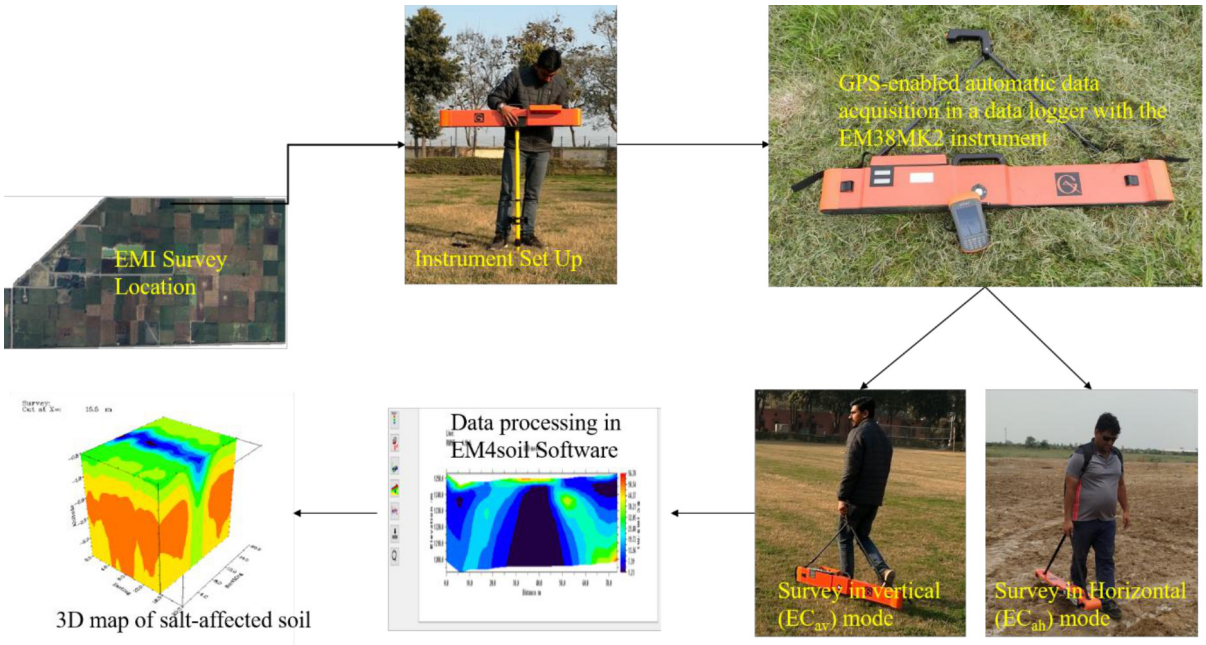

Fig. 3 The process flowchart of ECa measurement in the field using EM38MK2 electromagnetic induction sensors and 3D map generation using EM4Soil

Table 1. Descriptive statistics of Apparent conductivity (EC_a) in vertical and horizontal mode in 1 m and 0.5 m depth response measured through EM38MK2 and Electrical conductivity of soil saturation extract (dS m^{-1})

Parameters	n	Mean	SD	Minimum	Maximum	Skewness	Kartosis
Block 1 (Non-continuous dewatering)							
EC_{av}(1m)	52	135.7	14.2	35.5	496.4	2.5	7.7
EC_{av}(0.5m)	52	122.7	12.0	26.7	486.9	2.0	5.6
EC_{ah}(1m)	52	133.3	14.3	32.4	511.1	1.9	4.1
EC_{ah}(0.5 m)	52	106.6	13.3	16.1	467.6	2.2	5.5
EC_e (0-15 cm)	10	12.9	4.8	2.9	36.5	2.3	5.8
EC_e (15-30 cm)	10	8.6	2.3	2.9	25.6	2.3	5.9
EC_e (30-60 cm)	10	7.5	1.8	2.1	18.8	2.2	5.7
EC_e (60-90 cm)	10	8.3	2.3	3.3	20.2	2.0	4.2
Block 2 (Continuous dewatering)							
EC_{av}(1m)	46	134.6	12.7	59.8	618.0	3.2	13.6
EC_{av}(0.5m)	46	102.9	9.5	39.3	338.3	1.9	3.9
EC_{ah}(1m)	46	114.1	12.6	54.0	565.0	3.6	17.0
EC_{ah}(0.5m)	46	78.0	9.3	10.9	407.2	3.6	16.8
EC_e (0-15 cm)	6	11.3	3.1	4.1	28.9	0.9	-1.8
EC_e (15-30 cm)	6	8.7	2.1	2.3	17.1	0.6	-0.8
EC_e (30-60 cm)	6	6.9	1.5	3.2	15.0	1.0	0.7
EC_e (60-90 cm)	6	7.3	1.7	2.8	17.0	0.7	-0.8

from the soil profile and makes the root zone salt-free (Narjary *et al*., 2024, Kumar *et al*., 2020) in continuously operated drainage block (B2). Whereas, under non-continuous SSD operation in block B1, the removal of salts from the crop root zone was ineffective, leading to higher salinity levels and greater apparent conductivity compared to the continuously operated SSD block B2. In both the vertical and horizontal mode of orientation, standard deviation (SD) of apparent conductivity (EC_{av} and EC_{ah} in 1 and 0.5 m depth response) was less in B2 than in B1. These indicate that continuous reclamation process through SSD reduces soil salinity in all layers, and spatial variability of apparent conductivity is reduced.

Descriptive statistics of electrical conductivity (EC_e) from 16 calibrating sites (10 sample sites in B1 and 6 sample sites in B2) were consistent with the survey data set. Survey results indicated that increase in EC_e was accompanied by higher EC_a values in both vertical and horizontal modes. This suggests calibration data as a true representative of the survey data set. Electrical conductivity of saturated soil extract (EC_e) in B1 was in the range of 2.9-36.5 dS m^{-1} at 0-15 cm soil layer, 2.9-25.6 dS m^{-1} at 15-30 cm soil layer, 2.1-18.8 dS m^{-1} at 30-60 cm soil layer and 3.3-20.2 dS m^{-1} at 60-90 cm soil layer. Whereas at continuous SSD operated site (B2), EC_e was in the range of 4.8-28.9 dS m^{-1} at 0-15 cm soil layer, 2.3-17.1 dS m^{-1} at 15-30 cm soil layer, 3.2-15 dS m^{-1} at 30-60 cm soil layer and 2.8-17 dS m^{-1} at 60-90 cm soil layer. The mean soil salinity of B2 at all the layers (0-15, 15-30, 30-60, and 60-90 cm) was lower than B1. This is primarily due to the implementation of sub-surface drainage (SSD) leads to a significant reduction in soil salinity throughout the entire soil profile (Zhu *et al*., 2022; Mukhopadhyay *et al*., 2023) and is more prominent where sub-surface drainage operates continuously (Kumar *et al*., 2020).

Estimation of soil salinity (EC_e) at all depth increments from modelled true apparent conductivity (σ) data

In the present study, 3D inversion algorithm (EM4Soil v4 inversion software package, EMTOMO, 2020) was used to estimate the true electrical conductivity (σ, mS m^{-1}) from EC_{av} (1 m), EC_{av} (0.5 m), EC_{ah} (1 m) and EC_{ah} (0.5 m) apparent conductivity data. The calibrated parameters for developing the model are presented in Table 2, and the calibrated relationship between EC_e and σ are presented in Table 3. The developed model equation is

Table 2. The inverse modelling parameters used for the study site

Parameter	Study site (Kahni)
Dumping Factor	1.5
No of iteration	10
Inversion calculation	IS
Data error	1
Misfit target	0.2
Modelling Algorithm	Algotithm-S1
Layers	3 (0-30, 30-60 and 60-90 cm)
Solution	cumulative function

which signifies very good agreement between measured and predicted EC_e. Considering the whole range of measured EC_e (1.78-36.5 dS m^{-1}), the RMSE is acceptable (5.03 dS m^{-1}), indicating that overall prediction precision was good. However, the predicted EC_e of 0-15 cm soil layer positioned lower side of the straight line of Lin's concordance indicated under-fitting of the predicted EC_e. Working in waterlogged salt affected soil in Haryana, India, Koganti *et al.* (2018) got similar RMSE (8.31 dS m^{-1}) and Lin's concordance (0.93) between observed and predicted EC_e measured through the Dualem instrument. In salt-affected soil of Khon Kaen, Thailand, Khongnawang *et al.* (2022) also achieved a similar RMSE and Lin's concordance. These findings, which corroborate the findings of other researchers, indicate that the developed model was effective and is suitable for producing 3D soil salinity maps.

Table 3. Statistical summary of the model established between the calculated true electrical conductivity (s = mS m^{-1}) and measured electrical conductivity of the saturated soil paste extract (dS m^{-1})

	Coefficients	Standard Error	t Stat	P-value	R^2	Developed model
Intercept	1.024	0.79	1.3	0.20093	0.7075	$EC_e = 1.024 + 0.0460\ \sigma$
s	0.0460	0.0034	12.25	<0.00005		

$$EC_e = 1.024 + 0.0460\ \sigma \ldots (Eq\ldots1)$$

with a regression coefficient (R^2) of 0.71. The model is statistically significant with p value <0.00005. The model predicted EC_e was cross-validated with observed EC_e (Fig. 4). The outcome showed that quasi-3d model's predicted EC_e and the measured EC_e were found to be satisfactorily good for modelling. The high R^2 (0.71), low RMSE (5.03 dS m^{-1}), and large Lin's concordance (0.84),

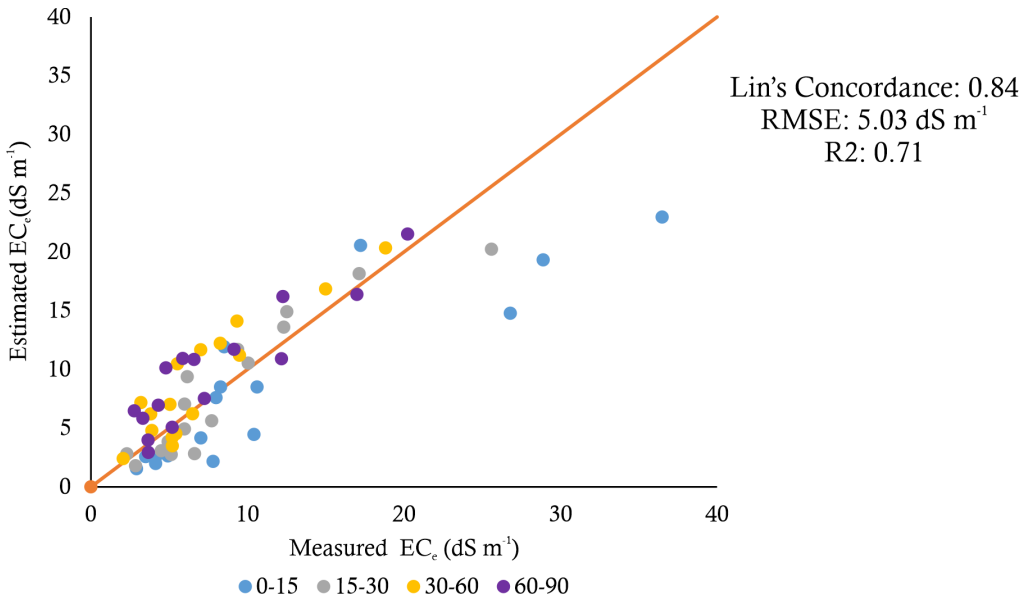

Fig. 4 Plot of validation results (R^2, RMSE and Lin's Concordance) achieved between measured EC_e (dS m^{-1}) and estimated EC_e (mS m^{-1}) generated by inverting EM38MK2 EC_a data (σ = mS m^{-1}) using the EM4Soil software across all depths.
(R^2 = coefficient of determination, RMSE = root mean square error, σ = inverted true electrical conductivity)

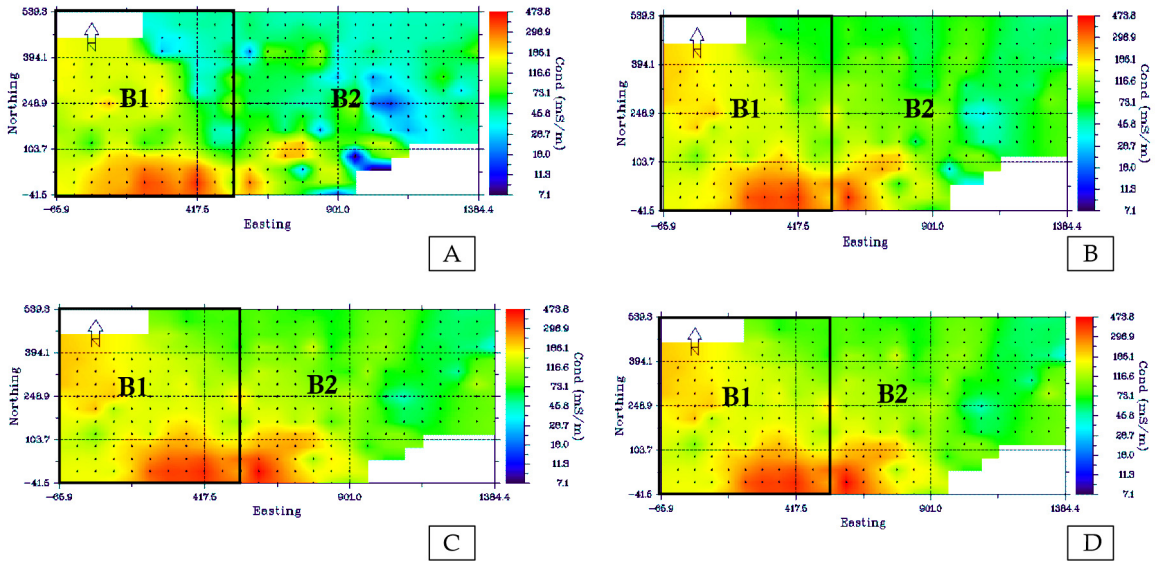

Fig. 5 Horizontal true apparent conductivity (σ: dS m^{-1}) distribution (A) 0-15 cm soil layer, (B) 15-30 cm soil layer, (C) 30-60 cm soil layer (D) 60-90 cm soil layer in B1 and B2 of the study area

Spatial distribution of soil salinity

Model-derived true electrical conductivity values (σ) showed strong spatial variability at surface (0-15 cm), subsurface (15-30 and 30-60 cm), and subsoil (60-90 cm) layers (Fig. 5) in both SSD blocks (B1 and B2). In B1, where dewatering of drainage effluents was non-continuous, the average soil σ was higher at the surface soil layer (0-15 cm) (108.3 mS m^{-1}) than B2 (continuous dewatering of drainage effluent) (71.5 mS m^{-1}). It was observed that soil salinity was higher in the deeper soil layer than the surface soil layer in both B1 and B2. This is mainly due to the dewatering of drainage effluents leach down the salt from the upper surface soil layer and depositing it in the lower soil layer. Both blocks were in a reclamative phase, and possibly groundwater existed at shallow depths. This shallow groundwater is also saline (Boumans *et al.*, 1988) in nature, resulting in higher salinity in the deeper layer (Askri *et al.*, 2022). In all layers (0-15, 15-30, 30-60 and 60-90 cm) soil salinity was more in B1 than B2. This was mainly due to, continuous dewatering from sub-surface drainage systems (SSD) can effectively remove salts from soil layers, thereby reducing salinity in the root zone (Christen and Skehan, 2001; Yang *et al.*, 2022). In B2, upper surface soil layer (0-15 cm) showed stronger spatial variability (Fig. 5) and two distinctive reclaimed zones (σ < 30 mS m^{-1}, corresponding EC_e <2 dS m^{-1}) were observed. Similarly, the higher σ values in B1 (σ > 200 mS m^{-1} corresponding ECe >8 dS m^{-1}) in all the soil layers may be attributed to inadequate dewatering through the SSD system. It was observed that a prominent low (headend: Upper elevation) to high soil salinity gradient (low end: near the sump) existed in B2. These distinctive features of soil salinity gradient were observed in most reclamative phase SSD systems. Narjary *et al.* (2024) reported that reclamation occurs at the final stage in the sump area of the SSD block, where drainage effluent is dewatered.

3D Vertical distribution of soil salinity

Model-derived true electrical conductivity values (σ) were used to describe and quantify the 3D vertical distribution of soil salinity (Fig. 6). 3D soil salinity map showed the spatial and profile (0-90 cm) distribution of salt in the soil profile. Figure 6a represents the total surveyed study area (B1 and B2). It was observed that the lowest soil salinity was at the surface (Fig. 6a), mainly in the part of B2. Patches of salt accumulation were observed beyond 60 cm soil layer. This is mainly due to the continuous operation of SSD in B2 leached down the salt from the upper surface and concentrates at the lower soil layer. Figure 6 b represents the 3D soil salinity distribution of total B1 and half of the area of B2. In this part of B2, soil salinity was lowest, and salinity continuously

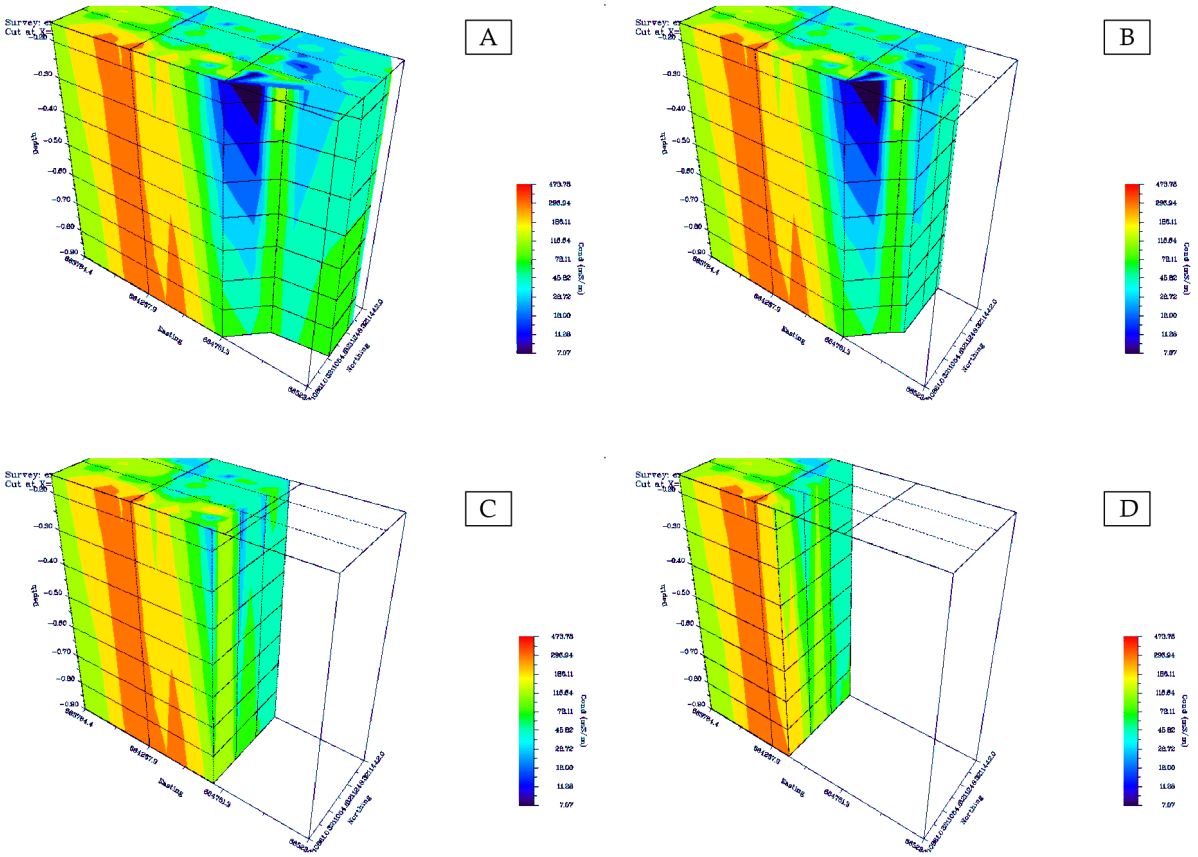

Fig. 6 3D true apparent conductivity (σ: mS m^{-1}) distribution (0- 90 cm) (A) Total B1 and B2, (B) Total B1and half of B 2, (C) Total B2 (D) Total half of B2 of the study area

increases with depth. The maximum area of SSD reclamation was clearly visible in this portion of B2. Based on the inversion data, the top soil (0-30 cm) and the middle layer (30-60 cm) in B2, had low salinity ranges (7-150 mS m^{-1}) and were classified as non-saline to slightly saline ranges (Narjary *et al.*, 2021). Similarly, the 60-90 cm soil layer with σ values between 150 mS m^{-1} and 250 mS m^{-1} was classified as moderately saline (Narjary *et al.*, 2021). The gradual increasing trend with depth (Fig. 6a-6d) clearly showed the effect of salt leaching from the upper soil layers in SSD reclamation process and the accumulation of salt in deeper layers (Narjary *et al.*, 2024).

Unlike the continuous SSD operated block (B2), the partial operated SSD block (B1) had much higher salinity values in both the surface and sub-surface layers (Fig. 6 c). Both the top (0-15 cm) and middle (15-30) soil layers had σ values of 150-450 mS m^{-1} and classified as 'slightly saline to extremely saline category. In B1, most of the deeper soil layer was highly to extremely saline. These show that the overall success of SSD depends on how effectively the dewatering of drainage effluents occurs from SSD blocks. Bundela *et al.* (2020) reported that effective pumping of drainage effluents is the key to the success of any SSD implemented project.

Summary and Conclusion

This study aimed to map and understand the three-dimensional (3D) distribution of soil salinity in a sub-surface drainage (SSD) site using electromagnetic induction (EMI) techniques and inversion modeling. Traditional soil salinity mapping is usually limited to two dimensions, lacking depth-wise information critical for effective land management. In this study, soil apparent electrical conductivity (EC_a) was measured using the EM38MK2 device in both vertical and horizontal orientations at 0.5 m and 1 m depths, across two experimental blocks: Block 1 (B1, non-continuous SSD operation) and Block 2 (B2, continuous SSD operation). This study

confirms the efficacy of electromagnetic induction (EMI) and 1D inversion modeling for generating 3D soil salinity maps, which provide a comprehensive understanding of both horizontal and vertical salinity distribution. Continuous SSD operation plays a critical role in effective salt removal, as evidenced by lower salinity and reduced spatial variability in B2. The developed model demonstrated strong predictive performance, supporting its application for salinity estimation over large areas. The 3D salinity maps revealed important spatial trends, such as top-to-bottom salt migration in reclaimed areas and significant sub-surface salt accumulation in poorly drained blocks. These insights are crucial for guiding future reclamation strategies, optimizing drainage designs, and achieving Land Degradation Neutrality (LDN) goals through targeted soil management interventions. Overall, the study highlights the potential of EMI-based 3D salinity mapping as a robust, cost-effective, and non-destructive approach for soil salinity monitoring and precision land management.

Acknowledgement

The authors are grateful to the DST SERB for providing financial assistance for undertaking this investigation under DST SERB Grant No EEQ/2019/000236. The authors are also grateful to the Director, ICAR-Central Soil Salinity Research Institute, Karnal, India, for extending logistical support during the execution of this study.

Conflict of Interest Statement

It is declared that the authors do not have any conflicts of interest in this publication.

Data Availability Statement

All data used in this study will be available upon reasonable request from the corresponding author.

References

Askri B, Khodmi S and Bouhlila R (2022) Impact of subsurface drainage system on waterlogged and saline soils in a Saharan palm grove. *Catena* **212**: 106070. https://doi.org/10.1016/j.catena.2022.106070

Boumans JH, van Hoorn JW, Kruseman GP and Tanwar BS (1988) Water table control, reuse and disposal of drainage water in Haryana. *Agricultural Water Management* **14**: 537-545. https://doi.org/10.1016/0378-3774(88)90103-5

Bundela DS, Pathan AL, Narjary B, Raju R and Sharma PC (2020) Operational Ranking of Subsurface Drainage Projects in Haryana and Suitable Interventions for Improving the Project Operational Performance. *Journal of Soil Salinity and Water Quality* **12(2)**: 187-197.

Carter MR and Gregorich EG (Eds.) (2008) Soil sampling and methods of analysis (2nd ed.). CRC Press.

Christen E and Skehan D (2001) Design and Management of Subsurface Horizontal Drainage to Reduce Salt Loads. *Journal of Irrigation and Drainage Engineering* **127**: 148-155. https://doi:10.1061/(ASCE)0733-9437(2001)127:3(148)

FAO (2024) Global status of salt-affected soils – Main report. Rome. https://doi.org/10.4060/cd3044en

Geonics Limited (2016) EM38-MK2 Ground Conductivity Meter Operating Manual. pp1-44. https://geophysicalequipmentrental.com/files/2020/01/EM38-MK2-Operating-Manual.pdf

Hassani A, Azapagic A and Shokri N (2021) Global predictions of primary soil salinization under changing climate in the 21st century. *Nature Communications* **12**: 6663. https://doi.org/10.1038/s41467-021-26907-3

Jiang Q, Peng J, Biswas A, Hua J, Zhao R, He K and Shi Z (2019) Characterising dryland salinity in three dimensions. *Science of the Total Environment* **682**: 190–199. https://doi.org/10.1016/j.scitotenv.2019.05.037

Khongnawang T, Zare E, Srihabun P, Khunthong I and Triantafilis J (2022) Digital soil mapping of soil salinity using EM38 and quasi-3d modelling software (EM4Soil). *Soil Use and Management* **38**: 277–291. https://doi.org/10.1111/sum.12778

Koganti T, Narjary B, Zare E, Pathan AL, Huang J and Triantafilis J (2018) Quantitative mapping of soil salinity using the DUALEM-21S instrument and EM inversion software. *Land Degradation and Development* **29**: 1768–1781. https://doi.org/10.1002/ldr.2973

Kumar S, Narjary B, Kumar V, Vivekanad, Prajapat K and Bundela DS (2020) Subsurface drainage improves physico-chemical conditions of rhizosphere for sustainable crop production in waterlogged saline soil – a case study. *Journal of Soil Salinity and Water Quality* **12(2)**: 213–224.

McNeill JD (1990) Geonics EM38 Ground Conductivity Meter: EM38 Operating Manual. Geonics, Mississauga, Ontario, Canada.

Mukhopadhyay R, Fagodiya RK, Narjary B, Barman A, Prajapat K, Kumar S, Bundela DS and Sharma PC (2023) Restoring soil quality and carbon sequestration potential of waterlogged saline land using subsurface drainage technology to achieve land degradation neutrality in India. *Science of The Total Environment* **885**: 163959. https://doi.org/10.1016/j.scitotenv.2023.163959.

Narjary B, Kumar S, Meena M, Kamra S K and Sharma DK (2021) Spatio-temporal mapping and analysis of soil salinity: an integrated approach through electromagnetic induction (EMI), multivariate and geostatistical techniques. *Geocarto International* **37(25)**: 8602–8623. https://doi.org/10.1080/10106049.2021.2002952

Narjary B, Nand V, Goswami S, Prajapat K, Bundela DS and Kumar S (2024) Restoration of degraded waterlogged saline soil through subsurface drainage: Spatiotemporal soil salinity assessment using electromagnetic induction (EMI) and geographic information system (GIS) techniques. *Land Degradation and Development* **35(12)**: 3790–3801. https://doi.org/10.1002/ldr.5167

Petsetidi P A and Kargas G (2023) Assessment and Mapping of Soil Salinity Using the EM38 and EM38MK2 Sensors: A Focus on the Modeling Approaches. *Land* **12(10)**: 1932. https://doi.org/10.3390/land12101932

Poggio L and Gimona A (2017) 3D mapping of soil texture in Scotland. *Geoderma Regional* **9**: 5-16. https://doi.org/10.1016/j.geodrs.2016.11.003.

Vibhute SD, Kamra SK, Pathan AL, Bundela DS, Abhishek R, Kumar S and Kumar J (2024) Rapid Assessment and Mapping of Soil Salinity in Subsurface Drainage Project using Electromagnetic Induction and Geostatistical Analysis. *Journal of Soil Salinity and Water Quality* **16(2)**: 249-256

Vineeth TV, Vibhute SD, Ravikiran KT, Prasad I, Chinchmalatpure A and Sharma PC (2023) Biosaline agriculture and efficient management strategies for sustainable agriculture on salt affected Vertisols. In *Plant Stress Mitigators* (pp. 249-269). Academic Press.

Yadav RK, Meena MD, Chaudhary M, Gajender, Rai AK and Sharma DK (2015) Laboratory Manual on Poor Quality Water Analysis. Technical Manual: CSSRI/Karnal/2015/2, pp.50

Yang Y, Li D, Huang W, Zhou X, Li Z, Dong X and Wang X (2022) Effects of Subsurface Drainage on Soil Salinity and Groundwater Table in Drip Irrigated Cotton Fields in Oasis Regions of Tarim Basin. *Agriculture* **12(12)**: 2167. https://doi.org/10.3390/agriculture12122167

Zare E, Huang J, Monteiro Santos FA and Triantafilis J (2015) Mapping salinity in three dimensions using a DUALEM-421 and electromagnetic inversion software. *Soil Science Society of America Journal* **79**: 1729–1740.

Zhang Y, Ji W, Saurette DD, Easher TH, Li H, Shi Z, Adamchuk VI and Biswas A (2020) Three-dimensional digital soil mapping of multiple soil properties at a field-scale using regression kriging. *Geoderma* **366**: 114253. https://doi.org/10.1016/j.geoderma.2020.114253.

Zhu H, Wu W, Jiang Q, Ren T and Liu P (2022) Effects of Subsurface Drainage on Soil Salinity and Groundwater Table in Drip Irrigated Cotton Fields in Oasis Regions of Tarim Basin. *Agriculture* **12(12)**: 2167.

Received: June 28, 2025; Accepted: October 15, 2025